Chitosan stimulates root hair callose deposition and inhibits root hair growth

Matěj Drs[1,2], Samuel Haluška[1,2], Eliška Škrabálková[1,2], Pavel Krupař[2], Lucie Brejšková[1], Karel Muller[1], Natalia Serrano[1], Andrea Potocká[1], Aline Voxeur[3], Samantha Vernhettes[3], Jitka Ortmannová[1], George Caldarescu[2], Matyáš Fendrych[2], Martin Potocký[1], Viktor Žárský[1,2], Tamara Pečenková[1,2*]

[1] Institute of Experimental Botany of the Czech Academy of Sciences, Rozvojová 263, 165 02, Prague 6, Czech Republic

[2] Department of Experimental Plant Biology, Faculty of Science, Charles University, Viničná 5, 128 44, Prague 2, Czech Republic

[3] Université Paris-Saclay, INRAE, AgroParisTech, Institut Jean-Pierre Bourgin (IJPB), 78000, Versailles, France

*corresponding author pecenkova@ueb.cas.cz

Abstract

Although angiosperm plants have a general capacity to react after the immunity elicitor chitin or chitosan treatment by the cell wall callose deposition, this response in particular cell types and its evolutionary conservation is not understood. Here we show that also the growing root hairs (RHs) of Arabidopsis can respond to a mild (0.001%) chitosan treatment by the callose deposition and by a deceleration of the RH growth. We demonstrate that the glucan synthase-like 5 (GSL5)/PMR4 is vital for chitosan-induced callose deposition but not for RH growth inhibition. Upon the higher chitosan concentration (0.01%) treatment, RHs do not deposit callose, while growth inhibition is prominent. To understand the specificities of the low and high concentration chitosan treatments, we analysed the PTI signalling components, gene expression, and RH cellular endomembrane and cytoskeleton modifications upon these treatments. Importantly, chitosan-induced callose deposition is also present in the functionally analogous and evolutionarily only distantly related RH-like structures rhizophores (lycopod) and rhizoids (bryophytes). Our results point to the RH callose deposition as a conserved strategy of soil-anchoring plant cells (rhizoids/rhizophores/RHs) to deal with mild biotic stress. At the same time, high chitosan concentration prominently disturbs intracellular dynamics, tip-localised endomembrane compartments and RH growth, precluding callose deposition.

Introduction

Root hairs (RHs) are unicellular plant structures crucial for several aspects of root function: mechanical anchorage of a plant in a substrate, the absorption of water and essential nutrients due to increased root surface, and in root-microbe interactions. In the model plant *Arabidopsis thaliana*, RH cell fate is determined by a position-dependent signalling cascade governed by specific transcription factors, leading to the RH initiation, bulging and cylindrical/polarised tip growth (Carol and Dolan, 2002; Dolan, 1996; Parker et al., 2000; Vissenberg et al., 2020). Several root hair-defective (RHD) genes, F-actin cytoskeletal meshwork and secretory pathway play a prominent role in this process (Baluška et al., 2000; Ichikawa et al., 2014). The tip growth is supported by constant modification of the preexisting cell wall (CW), as documented by the vital importance of several cellulose and hemicellulose biosynthesis participants (Cavalier et al., 2008; Park et al., 2011).

In aerial plant parts, when a pathogen attacks the plant cell, pathogen-associated molecular patterns (PAMP) triggered immunity (PTI) and potentially effector-triggered immunity (ETI) are activated (Jones and Dangl, 2006; Ngou et al., 2021). One of the earliest defence responses to a pathogen attack is the deposition of β-1,3 glucan polysaccharide callose by which the plant reinforces cell walls and blocks the pathogen entry (Jacobs et al., 2003). In Arabidopsis, among 12 callose synthase genes, only one of them, *GSL5* or *PMR4* (*POWDERY MILDEW RESISTANT 4*), is expressed upon pathogenic infection or elicitor treatment, such as fungal cell wall derived chitin and chitosan, but also endogenous damage-associated patterns (DAMP)(Denoux et al., 2008; Gómez-Gómez et al., 1999; Luna et al., 2011; Verma and Hong, 2001; Vogel and Somerville, 2000). It has been recently shown that this callose synthase is responsible also for the root hair callose deposition upon phosphate starvation (Okada et al., 2023).

In contrast to shoots, the roots are constantly exposed to a mixture of microorganisms, and plants need to prevent the over-activation of immunity in roots, mainly by restricting defence responses to specific root zones and cell layers (Chuberre et al., 2018). The PTI in roots also comprises the ROS production, sporadic and patchy callose deposition and growth rate modifications upon PAMP stimulation (Badri et al., 2008; Chuberre et al., 2018; Millet et al., 2010; Rich-Griffin et al., 2020; Zhang et al., 2022). Upon injury of RH, callose can be deposited locally in the RH cell wall as well, however, the identity of the callose synthase involved remains unknown (Galway et

al., 2011). The RH can react to pathogenic bacteria (e. g. *Pseudomonas syringae*), similarly to the beneficial ones, by the enhancement of the RH growth (Pečenková et al., 2017; Zamioudis et al., 2013). Unlike living bacteria, elicitor treatments in Arabidopsis did not provoke prominent RH growth changes, except for the DAMP PEP1 (Okada et al., 2021).

Both RH tip growth and pathogen sensing are under the control of receptor kinases, which further modulate the homeostasis of ROS and Ca2+. In both development and defence, the ligands binding to the cognate receptors, leads to the activation of Ca2+ channels CYCLIC NUCLEOTIDE GATED CHANNELS (CNGCs) (Ladwig et al., 2015)) which produce transients with specific patterns, further transmitted to transcriptional reprogramming of defence (or symbiosis) (Yuan et al., 2017). Recent studies have reported that CNGC6, CNGC9 and CNGC14 are crucial for RH tip polar growth (Brost et al., 2019; Ladwig et al., 2015). A phosphorylation activation of mitogen-activated protein kinases (MAPK) cascade is another convergence point of signalling pathways. Root hair MAPK3/6 signalling cascade plays a role in the RH growth (Rentel et al., 2004), as well as in plant immunity (including chitin-activated defence), together with the second MAPK4-comprising cascade (rev. in (Zhang and Zhang, 2022)).

The simplest way to study defence responses is by applying a single PAMP or immunity elicitor such as chitin or its derivate chitosan. Chitin is an insoluble polymer of β-1,4-linked N-acetylglucosamine, which is in Arabidopsis recognized by a complex of receptor and co-receptors - Chitin Elicitor Receptor Kinase 1 (CERK1) and lysin motif receptor kinases 4 and 5 (LYK4 and 5) (Cao et al., 2014; Miya et al., 2007; Wan et al., 2012). The chitin recognition activates the production of chitinases by plants; to avoid this recognition and hydrolysis by chitinases, fungi secrete chitin de-N-acetylases to convert chitin to chitosan. Fully deacetylated polymer units can still activate Ca^{2+} signalling-related subset of cellular responses, independent of the CERK1/ROS/MAPK pathway, which in case of overactivation provokes cell death (Ye et al., 2020).

Chitosan is typically obtained from marine crustaceans´ chitin by chemical deacetylation (up to 90%) with molecular weights (Mw) ranging from oligo- (<5 kDa) to polysaccharides (70–100 kDa). Due to the protonation of glucosamine, chitosan molecules carry an overall positive charge. Chitosan functions as a PAMP (Iriti et al., 2006), but also as an antimicrobial factor causing intracellular ROS burst with subsequent oxidation of pathogen cell membrane fatty acids and plasma membrane

permeabilization (Lopez-Moya et al., 2017). Interestingly, high doses of chitosan in the rhizosphere of Arabidopsis, tomato or barley significantly arrest root development, probably via interference with auxin and gibberellic acid regulation or via activation of jasmonic (JA) and salicylic acid (SA) related genes in roots (Lopez-Moya et al., 2017; Suwanchaikasem et al., 2022).

In this report, we compare the elicitation of plant immunity with two different chitosan concentrations, low 0.001%, further referred to as LCC, and high (0.01% HCC), focusing on RH reactions. We bring evidence of the plant capability to adjust the RH rate growth, as well as to reinforce the RH cell wall by the callose deposition. The observed RH-specific effects are dependent on the chitosan concentration, but not its molecular size, and are present also in the functionally analogous but evolutionary non-related structures, namely rhizoids of the liverwort *Marchantia polymorpha* and rhizophores of the lycophyte *Selaginella uncinata*, as well as in the regenerating protoplasts of *Physcomitrium patens*. Further, on the subcellular level, we tested the responsiveness of RH endomembranes and cytoskeleton to chitosan treatments. To understand the impact of the chitosan treatments on overall plant growth and defence, we performed Ca^{2+} and MAPK signalling assays and RNAseq analysis, pointing to limited but significant changes caused by LCC, compared to HCC treatment. Out of these experiments, we could conclude that the RH callose deposition is the consequence of the mild biotic stress affecting the cells with the intensive growth rate, while the stronger biotic stress provokes almost immediate and more prominent tip-localised endomembrane changes and RH growth cessation. Our results thus reveal the unexpected aspects of the RH growth-defence trade-off, and set the basis for possible future modifications of the general plant resistance by mild and environmentally low-impact treatments.

Results

Chitosan treatment induces concentration-dependent root growth changes and callose deposition also in root hairs

When the 5-7 day-old *A. thaliana* seedlings in liquid medium were treated with several different concentrations of chitosan 0.0001% - 0.01%, 24 h post treatment we could observe the ectopic callose deposition in cotyledon leaves, but also in roots and RHs (Figure 1A). The patterns were dependent on used concentration - while LCC (0.001%) induced small callose deposits in leaves, no primary root growth inhibition

138 and prominent callose depositions in regions close to the root tips, the HCC (0.01%)
139 induced larger callose deposits in leaves, prominent primary root growth inhibition
140 and no callose in root hairs. Conversely, plants incubated with very low chitosan
141 concentration (0.0001%) were indistinguishable from the mock treatment by both the
142 lack of prominent callose deposition and no inhibition of the primary root growth
143 (Figure 1A, B). Given the striking response of RH to specific chitosan concentration
144 (LCC, 0.001%), we wondered if it is caused by the particular chitosan composition. We
145 therefore tested the effect of the same low concentration for several other chitosan
146 variants with different Mw, viscosity, and solubility. The observed effect on the callose
147 deposition along RH was consistent for all analysed chitosan variants but not for the
148 non-deacetylated chitin, confirming that the RH callose deposition is chitosan-specific
149 (Figure 2). When the seedlings were treated by LCC in distilled water, which does not
150 support the RH growth such as liquid 1/2MS, there was no callose deposition in RH,
151 pointing to the fact that the callose is deposited only in newly growing RH exposed to
152 chitosan (Supplementary figure 1A). Similarly, the application of HCC provokes
153 strong RH growth inhibition without observable RH callose deposition
154 (Supplementary figure 1B).

155 We could conclude that chitosan provokes specific responses in both above-
156 ground organs and root hairs, depending on the applied concentrations.

157

158 **Callose deposition is PMR4-dependent and uncoupled from the RH growth**
159 **inhibition**

160 In order to uncover the key players in the RH callose deposition, we decided to
161 analyse the RH modifications in the *gsl5/pmr4* mutant lacking the callose synthase
162 isoform responsible for the pathogen-induced callose deposition. The LCC-induced
163 callose deposition was completely abolished in the *pmr4* mutant (Figure 3A). Further
164 on, when using the GFP-tagged PMR4 construct (Sabol et al., in preparation), we could
165 observe a higher accumulation of PMR4 on the tip of the newly growing RH 4h after
166 the chitosan addition in comparison to the mock treatment (Figure 3B). Along with the
167 callose *pmr4* mutant, we tested *cals8-1,* which is involved in the biotic stress-related
168 regulation of plasmodesmatal permeability, as well as a range of secretory, defence-
169 related (including signalling co-receptor *bak1,* chitin receptor *cerk1*) and phytohormone
170 mutants, however, for all of them we found the RH callose pattern similar to the one
171 in WT/Col-0 (Supplementary figure 1C).

172 While the 24 h treatment by HCC completely arrested the growth of new RHs,
173 the LCC caused a gradual decrease in RH growth (Figure 3C), and we hypothesised
174 that it may be coupled with callose deposition and rigidification of RH cell wall.
175 However, the LCC-induced RH growth decline in the *pmr4* mutant that does not
176 deposit callose was similar to that of WT/Col-0 (Figure 3A). We also monitored both
177 callose deposition and root hair growth in WT after the LCC addition, showing that
178 the callose starts to accumulate already at 4h time point, while the average inhibition
179 of the root hair growth starts to be evident after 8h, reaching significant difference from
180 mock treatment approximately 12 h after addition of chitosan (Figure 3D). This
181 difference in the time course pattern further confirms the independence of the RH
182 growth decline and callose deposition.

183 The LCC-induced callose deposition in RHs is thus PMR4-dependent and
184 uncoupled from the mechanisms underlying slower RH growth.

185

186 **Low concentration chitosan treatment triggers weak PTI-related signalling**

187 We further wanted to uncover differences in general activation of PTI responses
188 between the LCC and HCC treatments. For that purpose, we first followed calcium
189 spiking using sensor R-GECO construct (Keinath et al., 2015) in a 20 min treatment of
190 seedlings by the two concentrations of chitosan. There was only a mild Ca^{2+} increase
191 in spiking in LCC treatment compared to HCC treatment, which triggered more
192 prominent peaks of intracellular Ca^{2+} increase (Figure 4A). Besides their intensity, the
193 two treatments also differ in their patterns and peaking time, evidencing early
194 specificity of the LCC versus HCC. Interestingly, despite the obvious employment of
195 the Ca^{2+} channels in chitosan sensing, *cngc* mutants have unaffected deposition of the
196 callose to the RH cell walls, indicative of higher importance of the CNGC-mediated
197 signalling for the RH growth than for the callose deposition (Supplementary figure
198 1C).

199 Additionally, we assayed another parallel early signalling PTI pathway, MAPK
200 activation, after the two chitosan concentrations 30 min long treatments. Similarly, a
201 western blot analysis of MAPK activation by phosphorylation (quantified as a ratio of
202 band intensities obtained for the phosphorylated part and whole pool MAPKs)
203 demonstrates significant MAPK activation in both cases. However, HCC causes a more
204 prominent effect on the MAPK signalling pathway than the LCC (Figure 4B). The

205 distribution of activation along the three tested MAPKs - MAPK3,6 and 4 was similar
206 for both treatments.

207 These results confirm that the LCC treatment, similarly to the HCC one,
208 activates PTI-related signalisation, nevertheless, the pattern and intensities of these
209 activations significantly differ.

210

211 **Chitosan modulates rapid calcium and endomembrane dynamics but not actin**
212 **cytoskeleton in growing root hairs**

213 Having shown distinct fast calcium responses after LCC and HCC treatment,
214 we next analysed the spatiotemporal details of the Ca^{2+} reporter R-GECO within the
215 RH cells. In mock treatment, the very tips of RH undergo constitutive pulsatile changes
216 of R-GECO signal intensity, while the atrichoblasts´ R-GECO pattern transiently
217 changes upon the buffer exchange during the mock treatment, and much more
218 prominently upon chitosan treatments (Figure 5A, Supplementary video).
219 Interestingly, upon both the LCC and HCC, a wave of R-GECO signal often starting
220 within 5-7 min at the RH tips and moving to the RH cell interior and further on through
221 trichoblast toward other root cells was observed (Figure 5B, Supplementary video).

222 We then tested if and how the chitosan-triggered early signalling event affects
223 the intracellular dynamics. We focused on well-growing RH close to the root tip, and
224 after applying mock, LCC and HCC treatments, we followed intracellular changes in
225 localisation and dynamics of vacuolar and cytoskeletal genetic markers, as well as
226 endocytic dye FM4-64 in a real-time approach (Figure 6). We monitored treated RH
227 for 0-30 minutes. First, we could observe an immediate and significant root hair
228 growth cessation in the case of HCC-treated seedlings, often accompanied by RH
229 damaging and bursting. In addition, for LCC we could also observe significantly lower
230 average growth rates. Nevertheless, out of the obtained data distribution, we could
231 conclude that in the case of this treatment, RH mostly either stop or prominently slow
232 down their growth, or they grow at rates similar to mock-treated root hairs (Figure
233 6A). Interestingly, the vacuolar dynamics does not follow the trend found for growth
234 and the RHs react to the two treatments contradictory – while LCC causes small and
235 insignificant enhancement in vacuolar dynamics, HCC impairs the vacuolar dynamics
236 in the RH tip area (Figure 6B). The cessation of vacuolar movement in the RH tip upon
237 HCC treatment may be related to observation obtained for the same treatment on the

238 enhanced FM4-64 dye accumulation in RH endocytotic/vesicular compartment,
239 probably as a consequence of collapsing endomembrane trafficking (Figure 6C).

240 Since vacuolar dynamics is often governed by the actin cytoskeleton, we tested
241 the effect of various chitosan concentrations on the organization and dynamics of
242 filamentous actin in RHs. Somewhat unexpectedly, there was no difference in the actin
243 organisation during the early response to chitosan, as dynamics of actin-decorating
244 fimbrin-GFP were indistinguishable among the mock, LCC, and HCC treated plants
245 (Supplementary figure 2).

246 The microscopical observations thus confirmed that the LCC, despite
247 provoking prominent changes in CW composition and RH growth inhibition in later
248 time points, does not impose a prominent stress that would disturb endomembrane
249 compartments in early time points. On the other hand, HCC treatment significantly
250 inhibits RH growth, rapidly affects calcium gradient and oscillations in RH tip, blocks
251 vacuolar dynamics and provokes accumulation of endocytotic/FM4-64 marked
252 compartment.

253

254 **Chitosan induces changes in gene expression and cell wall components**

255 To obtain a more general view on chitosan responses and to gain another insight
256 into distinct plant reactions to low and high chitosan treatment, we performed the
257 RNAseq analysis of liquid medium-grown Arabidopsis seedlings treated with mock,
258 LCC or HCC for 24h. The general responsiveness of plants to LCC is far less dramatic
259 than what is observed on the level of RHs, as only 58 differentially expressed genes
260 (DEGs) were identified for LCC, and 8507 for HCC, comprising participants of plant
261 PTI responses; most of the DEGs found for LCC are also present in the HCC DEG gene
262 set, while only 11 genes are specifically regulated by LCC (Table I; Supplementary
263 table I). Out of these 11 DEGs, 10 genes are downregulated, and only one, AtLRX6
264 (Leucine-rich repeat-extensin 6; AT3G22800), upregulated and found to belong to
265 leucine-rich repeat/extension-type proteins, reported previously to play a role in RH
266 growth. We have also identified genes which were differentially expressed in LCC and
267 HCC treatments - in contrast to HCC which upregulates their expression, LCC
268 downregulates (bottom 5 genes in the Table I). Interestingly, when the same LCC was
269 applied on mature rosette leaves, both RNAseq and cell wall composition analysis
270 revealed differences that are more prominent and more similar to expression patterns

271 provoked by other elicitor treatments (similarly to the HCC-treated seedlings;
272 Supplemental figure 3A).

273 The restricted number of DEGs provoked by LCC is in concordance with milder
274 Ca^{2+} and MAPK responses activation and with limited morphological changes
275 observed mainly on the level of newly growing RHs, implying that the RH callose
276 encasement is an effective but limited and localised strategy for the plant to overcome
277 mild biotic threats, and to proceed with undisturbed development.

278 Even though our results are centred around seedlings' roots reactivity to
279 chitosan, in order to obtain a more general view of the LCC impact on plants, we
280 analysed LCC-caused gene expression of adult rosettes, and we encountered the
281 results with those from the cell wall profiling of the LCC-treated rosette leaves
282 (Supplementary figure 4; (Voxeur et al., 2019)). Both analyses accordingly revealed the
283 affection of pectin synthesis and modification/methylation states upon LCC. We next
284 realised an enzymatic fingerprinting of the homogalacturonans and xyloglucans using
285 a commercial polygalacturonase and an endo-cellulase, respectively, from 5-weeks-
286 old Arabidopsis leaves treated in presence of mock and LCC. We analysed the
287 oligosaccharide produced by LC-MS (Paterlini et al., 2022). It revealed that LCC
288 treatment likely triggered the demethylesterification and acetylesterification since the
289 relative amounts of GalA4Me decreased and GalA3 Ac increased, respectively.
290 Chitosan treatment also modified the structure and composition of hemicellulose
291 building blocks. It remains to be further assessed whether, and how the CW
292 components modifications take part in the RH responsiveness to chitosan.

293

294 **Callose deposition is conserved in evolutionarily unrelated structures functionally**
295 **analogous to root hairs**

296 Because the callose deposition was preserved in all tested signalling and/or
297 secretory pathway mutants, we speculated that it is a robust reaction which might be
298 evolutionary conserved and present also in non-angiosperm plant lineages and their
299 stress responses. In a similar experimental setup with plants cultivated in the liquid
300 medium, we were able to induce the growth of the morphological structures
301 functionally analogous to root hairs, namely rhizoids in the liverwort *Marchantia*
302 *polymorpha* and the rhizophores of spikemoss *Selaginella uncinata*. When the plants
303 were treated for 24 h with LCC, *M. polymorpha* rhizoids growing out of an asexual
304 reproductive body gemma were enclosed by callose, similarly to rhizophore surface

305 cells of *S. uncinata* (Figure 7). Also, no callose depositions were detected in mock, while
306 HCC treatment prevented their appearance, mirroring the situation with RH of *A.*
307 *thaliana*.

308 We further verified if the relation of chitosan treatment and callose response can
309 also be established for different unicellular model – regenerating protoplasts derived
310 from the moss *P. patens* tip growing protonemal cells (Brejšková et al., 2021; Cove et
311 al., 2009). We could indeed observe a prominent callose deposition caused by LCC,
312 while HCC treatment had a deleterious effect on protoplast viability and regeneration
313 (Supplementary figure 4A). Interestingly, in contrast to *P. patens* regenerating
314 protoplasts, above-ground tissue-derived protoplasts of *A. thaliana* did not deposit
315 callose while regenerating in the presence of chitosan (Supplementary figure 4B).

316 These results confirmed that the potential of RH and RH-like structure to
317 deposit callose is an evolutionary old intrinsic feature. This capacity, however, may be
318 exclusive for the tissue derived from the non-aerial plant parts, exhibiting fast cellular
319 growth and newly generating the cell wall.

320

321 **Discussion**

322 In this work, we uncovered the RHs capability to perceive the chitosan as an
323 elicitor, and depending on its concentration, to deposit callose to the cell wall and/or
324 to inhibit RH growth. The two processes are not mutually dependent, and the two
325 studied chitosan concentrations, the low (LCC) and the high ones (HCC), may induce
326 plant responses that overlap in their quality and quantity, but also those which are
327 specific. We also demonstrate that the shift in treatment stringency toward the milder
328 concentrations of the stressor can reveal new defence- and development-related
329 phenotypes.

330 Phytopathological studies often deal with approaches involving high elicitor
331 concentrations necessary to provoke responses that could be easily observed and
332 quantified (Aslam et al., 2009; Luna et al., 2011). We speculate that the low chitosan
333 concentration (LCC, 0.001%), used in our study, imposes a mild biotic stress, which
334 young plants can sustain, and to which they react by the adjustments on the level of
335 RHs (as the most exposed cell type) by slowing down their growth rate and by
336 fortifying the cell wall with callose. Besides RHs, the LCC stimuli are also perceived
337 by other root parts and also above-ground organs, as our results from Ca^{2+} and MAPK
338 assays showed. Interestingly, prolonged LCC treatment had no impact on the growth
339 of young plants, and they are not affected in their further development, implying an

340 accommodation to these low chitosan concentrations, also observable in quenching of
341 early phases of Ca^{2+} spiking patterns. Our results thus point mainly to the quantitative
342 difference between the LCC and HCC treatments. Nevertheless, in agreement with
343 RNAseq and CW analysis, the *Pseudomonas syringae* susceptibility assays showed an
344 absolute enhancement of resistance of plants to bacteria when applied with LCC, thus
345 strengthening our hypothesis that the mild biotic stress provides an optimal score for
346 defence and growth trade-off costs (Supplementary figure 5A).

347 Similarly, the RNAseq data from LCC- and HCC-treated seedlings corroborate
348 the existence of primarily quantitative differences between the two treatments since
349 only a minority of DEGs was found to be specific for LCC. Nevertheless, the presence
350 of minor qualitative differences is legible as well. For instance, it has been reported
351 that the HCC treatment, which impairs plant growth, also affects the auxin pathway.
352 In contrast, LCC has only a minor effect on auxin signalling enhancement, as
353 demonstrated using the DR5::GFP auxin reporter line (Supplemental figure 5B).
354 Despite the scarcity of the LCC-specific candidates, we consider that the role of one of
355 the identified DEGs, LRX10, is worthy of further verification, since this protein,
356 together with related pollen tube-expressed isoforms, has been found to be involved
357 in the pollen tube cell wall pectins and callose deposition, important for the process of
358 fertilisation (Wang et al., 2018).

359 Callose deposition is typically described as an early defence response in leaf
360 tissue, where it serves mainly to seal the plasmodesmatal connection between cells to
361 prevent pathogen spread and nutrient withdrawal (Epel, 2009) or to prevent
362 pathogens' entrance (Meyer et al., 2009; Ortmannová et al., 2022)), but also in primary
363 root epidermis after the defence-eliciting treatments, displaying a similar spotty
364 pattern as found in leaves (Millet et al., 2010). In agreement with this defence
365 involvement, callose deposition is repressed in the establishment of mutualistic
366 interactions (rev. (German et al., 2023)). Besides the defence-related functions, callose
367 also serves as a mechanical support in the new cell wall formation, in the pollen exine
368 formation and germinating-pollen plug, but also in a functional specialisation of
369 trichome basal parts (Kubátová et al., 2019; Kulich et al., 2015; Ma et al., 2021;
370 Motomura et al., 2022). The RH callose deposition observed by us is tightly coupled
371 with a state of the elongating root cells, and in the newly growing root hairs in the
372 zones closest to the root tip. Therefore, we hypothesise that the RH callose coating is
373 the consequence of two processes going along – of the elicitor caused defence
374 signalling, as evidenced by the dependance on the typically pathogen-induced isoform
375 of callose synthase PMR4, but also of the fragile and immature state of the cell wall

undergoing synthesis, which was additionally confirmed on our experiments with regenerating protoplasts that readily deposit callose upon the LCC treatment (Dehors et al., 2019), as well on recently demonstrated abiotic stress and starvation related RH callose deposition (Okada et al., 2023).

Both LCC / HCC treated rhizoids/rhizophores of *Marchantia polymorpha* and *Selaginella uncinata*, despite their evolutionary unrelated origins, provide the same morphological and subcellular responses, including the employment of the evolutionarily conserved callose synthases in terrestrial plants. This functional conservation might have an origin in the callose contribution to the newly formed post-meiotic cell wall of spores or pollen. Secondarily, these independently-evolved mechanisms may have also been involved in the onset of responses of plant cells to the hostile environmental conditions of land plants, also including pathogen threat (Herburger and Holzinger, 2015; Ks et al., 2020).

Unlike LCC, the HCC has a prominent effect on the appearance and subsequent loss of complexity of the RH tip-localised portion of the vacuolar compartment. The HCC causes the vacuolar withdrawal and dismission of the complex tubular tip-localised vacuolar growing parts. Given the massive uptake of FM4-64 dye in HCC-treated RHs, this may be the consequence of the enlargement of the endocytic zone in the RH tip, or an unrelated endomembrane response. The prompt response of vacuolar dynamics to chitosan may suggest that, besides a proposed role for vacuolar calcium channels in mechanosensing of the tip-growing cells, a part of the pathogen sensing might reside on the tonoplast as well (Radin et al., 2021).

Despite the critical importance of the actin cytoskeleton in both RH growth and responsiveness to pathogens, in our experiment, at an early time points, there was no significant modification of fimbrin-GFP-labelled actin filaments upon chitosan treatments (Supplementary figure 3, see also (Porter and Day, 2016; Ringli et al., 2002; Sun et al., 2021; Vaškebová et al., 2018)). It would be interesting to verify if this observation might be related to the different requirements for the callose- and cellulose synthases localization along the plasma membrane by the microtubules and the actin, respectively, similarly to what has been found for the tobacco pollen tube (Cai et al., 2011).

In addition to demonstrating the usefulness of mild chemical/eliciting treatments of plants for opening new perspectives in plant studies, we are also suggesting the simple experimental setup based on a single, exposed, and sensitive cells. This approach could be further employed for gaining the knowledge on the root

411 and RH-related immunity, as well as in the studies of the overall plant fitness in
412 relation to the rhizosphere conditions.

413

414 **Conclusions**

415 The effect of the low concentration chitosan treatment on the callose
416 accumulation in Arabidopsis root hairs and similar effect in Marchantia and
417 Selaginella rhizoids or rhizophores, expose their unexpected deeply rooted capacity to
418 react by the callose accumulation in response to this fungal elicitor. The root hair cell
419 wall callose deposition is PMR4/GSL5-dependent and occurs in parallel, but
420 independently of the root hair growth inhibition. The higher chitosan concentration
421 treatments cause prominent root hair growth inhibition that precludes the callose
422 deposition, leading to the phenotypic difference between the two treatments. The
423 intensive root hair growth inhibition is probably the consequence of the emphatic
424 defence alerting, as well as interference with the root tip-localised vacuolar and
425 endocytic compartments.

426

427 **Material and methods**

428 **Plant cultivation**

429 For seedlings and plants cultivation, seeds were surface sterilised (5 min in 70%
430 ethanol, 2 × 5 min in 10% commercial bleach, rinsed three times in sterile distilled
431 water) and stratified for 2–3 days at 4°C. Seeds were then germinated and grown on
432 vertical ½MS agar plates (half-strength Murashige and Skoog salts, Duchefa
433 Biochemie, supplemented with 1% sucrose, vitamin mixture, and 1.6% plant agar,
434 Duchefa Biochemie) at 21 °C and 16 h of light per day for five-seven days. For
435 cultivation of plants, seedlings that were 7 d-old were transferred into Jiffy Products
436 International pellets and grown at 22 °C and 16 h of light per day in growth rooms.

437 The following previously published Arabidopsis mutant and transgenic lines
438 were used in this study: *aux1-21* (CS9584, (Bennett et al., 1996)), *bak1-4* (CS71777;
439 (Kemmerling et al., 2007)), *cals8-1* (SALK_037603; (Cui and Lee, 2016)), *cerk1-1*
440 (pst14772; (Miya et al., 2007)), *cngc14-1* (SALK206460; (Shih et al., 2015)), *cngc2-3*
441 (SALK_066908; Chin et al., 2013), *exo70H4-1* (SALK_023593;(Kulich et al., 2015)), *npr1*
442 (CS3726; (Cao et al., 1994)), *pmr4-1* (CS67159; (Vogel and Somerville, 2000)), *rbohD-3*
443 (N9555, Torres et al., 2002 11756663), UQ10::GFP-PMR4 (Kulich et al., 2018),

promPMR4::GFP-PMR4 (Sabol et al, in preparation), DR5-GFP (Heisler et al., 2005), fimbrin-GFP (Wang et al., 2004), and vacuolar ATPase Vti-GFP (gifted by Karen Schumacher, Heidelberg). The wild type (WT) Col-0 was used as control. When needed, primers used for the genotyping were the same as used in the above-cited original studies.

Chitosan treatment

Plants were propagated in vitro for 5-7 d on vertical plates, and then transferred by forceps into liquid ½ MS (control) or liquid ½ MS with chitosan added (100x and 1000x diluted stock solution of the 1% chitosan in 1% acetic acid), usually 4-8 plants per 3 ml, in 6-multiwell plates (Nunclon, Thermo Fisher Scientific). Plants were cultivated for 24 h 16/8 h light/dark at 21–22°C without shaking. After 24 h of incubation, plants were transferred to 3 ml of ethanol for 6-24 h at room temperature for destaining, with mild shaking, and subsequently transferred into 3ml of 150 mM K2HPO4. After 1h, aniline blue (final concentration 0,005% solution in 150 mM K2HPO4) was added and seedlings stained for additional 24 h with mild shaking and observed under the microscope. Additional verifications confirmed that there were no differences between the mock treatment with and without corresponding dilution of acetic acid. Several chitosans used for analyses were purchased from Merck, Germany (Cat. Nos C3646, 523682, 448877 and 419419), as well as chitin (C7170).

Root and root hair phenotype examination

The plant responses to pathogens were monitored by microscopy and documented by photography. The seedlings were placed on microscopic glass, their primary root stretched and lengths measured. Microscopic analysis of root tips and root hairs was performed using an Olympus BX51 microscope with attached DP50 camera (Olympus; Psm) or Zeiss AxioImager ApoTome2 microscope (Pst). For each treatment/genotype 5-10 plants were photographed and analysed. Root hair lengths were determined for the first 20-40 root hairs starting from the root tip for each plant; for statistical analysis. Callose deposition was analysed using the pre-set conditions for bright-field and DAPI and objective 5x or 10x.

Protoplasts preparation

The moss *Physcomitrium patens* Gransden strain was routinely propagated in vitro on BCD medium supplemented with ammonium tartrate dibasic (BCDAT), according to (Cove et al., 2009), in a climate chamber (16 h of light/8 h of dark, 25 °C, illuminated by fluorescent tubes at 50-70 μmol m^{-2} sec^{-1}). Protonemal tissue (6-7 days after propagation) from cellophane-grown culture was transferred into the

479 1%Driselase/8%mannitol solution. When filamentous structure became invisible
480 (approx. 1 h at RT), protoplast suspension was filtered via/through 100 μm steel mesh.
481 Protoplasts were diluted in 8% mannitol up to 10 ml and spun down (700 rpm for 4
482 min, without brake) and this step was repeated three times. Protoplast sediment was
483 carefully resuspended between centrifugations to avoid aggregation of protoplasts.
484 Finally protoplasts were incubated in the liquid regeneration medium (BCDAT+ 5mM
485 NH_4+ 6% w/v mannitol + 10 mM $CaCl_2$) overnight at RT. Arabidopsis protoplasts were
486 prepared according to (Yoo et al., 2007). Briefly, Arabidopsis leaves from 3-4 weeks old
487 plants grown under short day conditions (8 h og light per day) were cut onto 2 mm
488 stripes. The 2g of prepared plant tissue were submerged in 37 °C warm protoplast
489 solution (0.4M mannitol, 1.5% cellulase, 0.4% macerozyme, 20mM MES pH 5.7, 20mM
490 KCl, 0.1% BSA, 10mM CaCl2) and vacuum has been applied for 30 min. The
491 submerged leaves were kept in the dark in RT. After 3 h, the flasks with protoplasts
492 were gently swirled and the quality of protoplasts was checked with a microscope.
493 The protoplast solution was washed with a WI buffer (4mM MES pH 5.7, 0.5M
494 mannitol, 20mM KCl), filtered through miracloth and clarified with multiple
495 centrifugations (3x100g, 2 min). For the recovery of protoplasts, 0.7 ml of WI solution
496 in a 12-well plate was applied. Both types of protoplasts were left to recover for 3h,
497 and were subsequently treated with chitosan or mock for 24 h. Protoplasts were
498 stained with aniline blue and the final condition of protoplasts monitored with the
499 microscope Olympus BX51 microscope with attached DP50 camera.

500 **Selaginella and Marchantia propagation and callose deposition assay**

501 For sterile *Selaginella uncinata* ('Comenius' strain) culture establishment, excised
502 fragments containing meristems were washed with distilled H_2O and surface sterilized
503 with 70% EtOH (1 minute) and subsequently with 40% commercial bleach (SAVO)/2%
504 sodium hypochlorite for 15 minutes and rinsed with a sterile water twice (Park et al.,
505 2020) . Axenic regenerants were subsequently vegetatively propagated on ½ MS media
506 with 0.6% agar under standard conditions (22°C, 16/8 light/dark, ca. 180 μmol/m^2/s).
507 Chitosan treatments were performed on whole regenerating plantlets interchangeably
508 with the *Arabidopsis thaliana* approach.

509 *Marchantia polymorpha* Tak-1 has been maintained on ½ Gamborg media
510 ((Gamborg et al., 1968) ; G0210 Duchefa) supplemented with 1,2% agar under standard
511 conditions (22°C, 16/8 light/dark, ca. 180 μmol/m^2/s). Chitosan treatments were done
512 with gemmae analogously to an *Arabidopsis thaliana* procedure, with a slight change,
513 where the liquid ½ MS has been replaced with ½ Gamborg media supplemented with
514 1% sucrose to enhance the rhizoids initiation.

515 **Confocal and Real Time microscopy**

516 Small agar block with *in vitro* cultivated 6-day-old seedlings was gently cutted
517 from the cultivation plate and transferred into sterile microscopic chambers containing
518 100 ul of liquid ½ MS. Chambers were covered with lids and left overnight in a
519 cultivation chamber. For real time treatments we used custom designed 3D printed
520 perfusion add-on which fits into the microscopic chamber and allows exchange of
521 media inside the microscopic chamber during microscopy session. To mediate the
522 exchange we used medical grade silicone tubes mounted onto a peristaltic pump and
523 perfusion add-on with speed approximately 100 ul/min. All microscopic samples were
524 10 min pretreated with the mock solution right before capturing, chitosan treatment
525 was applied directly during the microscopic session. For mock treatments the liquid
526 1⁄2MS was used. For chitosan treatments, 0.001% chitosan (LCC) or 0.01% chitosan for
527 HCC were added into the ½ MS. For the FM4-64 (Thermofisher scientific) staining we
528 used the same perfusion settings and solutions just with the addition of 0.001% FM4-
529 64 dye (1 mM stock solution). Samples were treated for 15 minutes before observation.

530 Real Time imaging was done on the Spinning disc (SD) microscope Nikon
531 (Eclipse Ti-E, inverted) with Yokogawa CSU-W1 SD unit (50mm) equipped with
532 Omicron LightHUB ULTRA light source, Plan-Apochromat L 20x/0.75 or Plan-
533 Apochromat LS 40x/1.25 WI objectives were used for capturing. Microscope is
534 operated by NIS Elements 5.30 software. GFP was observed using a 488 nm excitation
535 laser with Semrock brightline Em 525/30 filter. FM4-64 was observed using a 488 nm
536 excitation laser with Semrock brightline Em 641/75 filter.

537 **Analysis of vacuolar dynamics**

538 Dynamics of vacuoles were analysed using *stack difference* task inside *mutli*
539 *kymograph* plugin ImageJ (FIJI) followed by analysis of *moments* thresholded area of the
540 result image. See supplementary material *VD_macro.ijm.*

541 **FM4-64 uptake analysis**

542 Average Z projections of single RH were taken with subsequent analysis of
543 signal intensity within inner cell space (ImageJ - FIJI).

544 **Ca2+ signalling reporter imaging and evaluation**

545 *A. thaliana* seedlings expressing R-GECO1 Ca2+ signalling reporter were
546 vertically grown in a growth chamber at 23 °C by day (16 h), 18 °C by night (8 h), 60%
547 humidity and light intensity of 100 μmol photons m^{-2} s^{-1} (Keinath et al., 2015).
548 Microfluidics experiments were performed using four-day-old seedlings placed into a

549 microfluidic chip and enclosed by a cover glass (Serre et al., 2021). Channel one
550 contained a control solution (½MS, fluorescein dextran 6 µg/ml), while channel two
551 contained a treatment solution (½MS, 0.01% or 0.001% chitosan). The media flow rate
552 was 3 µl/min (OBI1, MFS2 Elveflow, and Elveflow software ESI (v.3.04.1). The system
553 was mounted to a vertical microscope stage and kept for 15 min plant recovery. The
554 media exchange was indicated by fluorescein-dextran signal intensity.

555 Plants were imaged using a vertical stage Zeiss Axio Observer 7 with a
556 Yokogawa CSU-W1-T2 spinning disk unit with 50-µm pinholes equipped with a VS-
557 HOM1000 excitation light homogenizer (Visitron Systems), objective Zeiss Plan-
558 Apochromat ×10/0.45. Images were acquired using VisiView software (Visitron
559 Systems, v.4.4.0.14). R-GECO1 was excited by a 561 nm laser, and fluorescein dextran
560 by a 488 nm laser. The signal was detected using a PRIME-95B Back-Illuminated
561 sCMOS camera (1,200 × 1,200 pixels; Photometrics). The seedlings were imaged every
562 13 s for 60 min. The signal intensity of R-GECO1 was measured inside the root at the
563 root late elongation zone using ImageJ Fiji software (Schindelin et al., 2012). The
564 intensity of the background was measured in areas not affected by the root response
565 and subtracted from the R-GECO1 values. The intensity of fluorescein-dextran was
566 measured outside of the root. The data were normalised using division by initial
567 fluorescence intensity values (F/F0). As the initial value F0, we used the average
568 fluorescence intensity at five-time points before treatment.

569 **RNA isolation and RNAseq analysis**

570 RNA was isolated from young, 6-7-day-old whole seedlings (transferred from
571 vertical 1/2MS plates to liquid ½ MS for treatments), and adult (5-6 week old) rosette
572 leaves of *A. thaliana* plants, using the RNeasy Plant kit (Qiagen) according to the
573 manufacturer's instructions. Isolated RNAs were stabilized by GenTegra technology
574 microtubes (GenTegra, Pleasanton, California, USA). Strand-specific cDNA libraries
575 were constructed from polyA enriched RNA and sequenced on the Illumina
576 NovaSeq6000 platform with subsequent analysis performed by Eurofins. The RNA-
577 seq data used in this study are deposited in the National Center for Biotechnology
578 Information Gene Expression Omnibus database.

579 **Protein extraction, western blot and MAPK assay**

580 Total protein extracts were isolated from 5–7-day-old *A. thaliana* seedlings
581 according to procedure described in Fernandez et al., 2020. Briefly, untreated and
582 chitosan treated tissue samples were ground in liquid nitrogen and dissolved in an
583 extraction buffer containing Phosphostop, and the concentration of proteins

584 determined by the Bio-Rad protein assay kit with BSA as the standard. The extracts
585 were denatured by boiling in 6× SDS loading buffer. The protein samples were
586 separated by 10% SDS-PAGE and analysed by Western blot using the α-p44/42-ERK
587 antibody (SAB4301578), anti-MAPK3 (M8318, Sigma), anti-MAPK4 (A6979, Sigma),
588 and anti-MAPK6 (A7104, Sigma). The primary antibodies were incubated with the
589 membranes for 3 h at room temperature in the blocking solution. Horseradish
590 peroxidase-conjugated antibodies (anti-rabbit and anti-mouse; Promega) were applied
591 followed by chemiluminescent ECL detection (Amersham) by the Bio-Rad
592 documentation system. Using the Gel Analysis function of ImageJ, signal intensities
593 for protein bands were determined for each treatment from 3 different samples.
594 Loading consistency was examined by staining the membrane with Ponceau S.

595 **Cell wall preparation and enzymatic fingerprinting**

596 For cell wall analysis plants have been propagated in Jiffy pellets for 5-6 weeks,
597 10/14 h of light/dark regime. Plants were treated by dipping into the mock (distilled
598 water with 0.005% Silwett) or LCC chitosan (distilled water with 0.005% Silwett and
599 0.001% chitosan), and left for 24 h in the growth chamber. Treated and non-treated
600 samples were submerged in 96% (v/v) ethanol and boiled at 70°C for 10 min. The
601 pellets were collected by centrifugation (13000 g for 10 min) and dried in a speed
602 vacuum concentrator at 30°C overnight. Samples were digested with 1 U/mg DW
603 sample of *Aspergillus aculeatus* endo-polygalacturonase M2 (Megazyme, Bray, Ireland)
604 (Paterlini et al., 2022) in 50 mM ammonium acetate buffer (pH 5) at 37 °C for 18 h.
605 Samples were centrifuged at 13000 rpm for 10 min and 100 µL of the supernatants were
606 transferred into vials. The oligosaccharides released from digestion were analysed
607 according to (Paterlini et al., 2022).

608 **Bacterial flooding assay**

609 Flooding assay was performed with modifications according to Ishiga et al.
610 2012 (Pečenková et al., 2020). Briefly, plants grown in vitro (½ MS, at 21°C, 12 / 12 h of
611 light / dark per day, for 10 -12 days) were pretreated with mock (water with 0.0025%
612 Silwet), or with chitosan (LCC, diluted in water with 0.0025% Silwet), both by flooding,
613 and decanting after 2 min. After 24 h, the *P. syringae pv. tomato* DC3000 (Pst) OD = 0.05,
614 was used for flooding for 2 min: the mock pretreated group was inoculated with either
615 chitosan and Pst (chit + Pst), or with Pst only, together with the chitosan pretreated
616 group (24 h chit + Pst) After the incubation, plants (three to four seedlings in one
617 sample, four samples for each line, in three replications) were homogenized,
618 homogenates subsequently diluted in series, plated put, and after approximately 36 h
619 of plates incubation on 28 °C colonies counted.

Image analysis and statistics

Image processing software was employed for image data quantification. Roots and root hair sizes were analysed using AnalySIS (Soft Imaging System GmbH, Germany) or ImageJ (Schneider et al., 2012) software. The numerical data obtained were processed using Microsoft Excel.

To determine statistical significance, Student's t-test and ANOVA tests were conducted either using Excel or on-line calculators (http://in-silico.net, and http://statpages.info/anova1sm.html). P-values of less than 0·05 indicated a significant difference among the various groups. For multiple-comparison experiments, the Tukey Honestly Significant Difference (HSD) post hoc test was used.

Contribution

M.D. performed root hair confocal microscopy, designed the experimental setup for the real time observation of root hairs, performed microscopy and image analysis, prepared RNA for RNAseq analysis, prepared figures and wrote the manuscript. S. H. performed Selaginella and Marchantia experiments, and wrote the corresponding parts in the manuscript. E. Š. performed MAP kinases assays. P. K. and M. F. performed Ca2+-spiking recording and analysis. L. B. and J. O. prepared protoplasts and analysed their cell wall. K. M. and N. S. analysed RNAseq data. A. P. performed Pst susceptibility assays. A. V. and S. V. did the cell wall fingerprinting analysis. G. C. verified callose deposition in mutant lines. M. P. and V. Ž. planned the experiments and wrote the manuscript. T. P. performed root hair growth and callose deposition analysis, prepared figures and wrote the manuscript.

Acknowledgment

We would like to thank to Norbert Zlámal from the Bratislava`s Comenius University Botanical Garden for sharing *Selaginella uncinata*, Adriana Jelínková and Edita Janková Drdová (IEB CAS) for sharing Arabidopsis mutants and markers seeds, and Jana Šťovíčková for technical assistance. This work was supported by the Ministry of Education, Youth and Sports project CZ.02.1.01/0.0/0.0/16_019/0000738, 8J19FR001 MEYS Czech-French mobility program and Charles University Grant Agency (GAUK) project 415322.

653 **Legend to figures**

654 **Figure 1.** Concentration dependent modes of chitosan-triggered callose deposition.
655 Different concentrations of chitosan cause different patterns of callose depositions 24
656 h post treatment (p. t.) in both cotyledons and roots (root hairs); mock treatment as a
657 control below (bar = 100 μm). B) Concentration dependent primary root growth
658 inhibition 24 h p. t. Small letters indicate significance of differences based on the
659 ANOVA test.

660 **Figure 2**. Root hair growth during the chitosan treatments. A) The low chitosan
661 concentration (0.001%, LCC) of several other chitosan variants has the same effect on
662 RH callose deposition (bar = 100 μm).

663 **Figure 3.** Callose deposition in LCC is PMR4-dependent. A) A *pmr4* mutant root hair
664 (RH) growth does not deposit callose upon the LCC treatment; nevertheless, the RH
665 growth is suppressed to the similar extent as in the Col-0 control. Small letters indicate
666 significance of differences based on the ANOVA test. B) Upon the LCC treatment, at 4
667 h p. t. GFP-PMR4 accumulates on the tips of growing RH, further confirming a role for
668 PMR4 in RHs callose deposition (marked by white asterisks). C) The time course of
669 decline of the RH growth during the LCC treatment; the significant growth inhibition
670 is observable at 12 h p.t. D) Timecourse of callose deposition reveals significant
671 changes between the mock and LCC already at 4 h p. t. Bars = 100 μm in A), C) and
672 D) and 10 μm in B).

673 **Figure 4.** Chitosan-triggered signalling in *A. thaliana* seedlings. A) Ca^{2+} spiking
674 analysed as R-GECO sensor fluorescence in root cells upon chitosan treatment shows
675 slightly later onset with mild oscillations and long duration within the ca 45 min frame
676 of LCC treatment, while HCC induces prominent Ca^{2+} spiking with subsequent drop
677 in signal intensity. B) Western blot analysis of MAPK activation by phosphorylation
678 upon 30 min of HCC and LCC treatments quantified as the ratio of band intensities
679 obtained for phosphorylated portion versus the whole pool MAPKs. Both treatments
680 cause significant increase in MPK3/6/4 phosphorylation in comparison to the mock
681 treatment, also the difference between the LCC- and HCC-caused phosphorylations is
682 significant, with LCC causing almost two-time less MAPKs phosphorylation.

683 **Figure 5.** R-GECO signal patterns upon mock, LCC and HCC treatment; below are
684 kymographs showing R-GECO dynamics within the selected RH (white rectangles in
685 upper row) in a time range of approximately 7 min after treatments; bars = 100 μm.

686 **Figure 6.** Subcellular dynamics during the early time points of LCC and HCC
687 treatments. A) The real-time analysis of the root hairs growth during the mock, LCC,

688 and HCC treatments based on the bright field images. The plot shows the RH growth
689 rates for the mock, LCC and HCC treatments; small letters indicate significant
690 differences based on Kruskal - Wallis test. B) The real-time changes in the vacuolar
691 dynamics quantified as a vacuole-occupied area in the RH tip, imaged using the
692 tonoplast marker Vti-GFP. The plot displays the differences between two consecutive
693 frames; the examples of the differential signal are shown on the right; examples of
694 vacuolar dynamics are shown below. Small letters indicate significant differences
695 based on the ANOVA test. Bar = 20 μm. C) The analyses of the endocytosed FM4-64
696 dye after 15 min of treatments for mock, LCC, and HCC. The endocytic compartment
697 stained by FM4-64 in the RH tip area is prominently enhanced in case of the HCC
698 treatments. Small letters indicate significant differences based on Kruskal -Wallis test.
699 On the right are examples of maximal intensity projections of FM4 -64 stained root
700 hairs. Bar = 10 μm.

701 **Figure 7.** Callose deposition is conserved in structures analogous to root hairs. *M.*
702 *polymorpha (liverwort)* rhizoids growing out of gemma are enclosed by callose when
703 incubated for 24 h with LCC. The same effect is observable also on spikemoss
704 rhizophores (*S. uncinata*). Bar = 100 μm.

705

706 **Table I.** Eleven genes (out of 58 DEGS; most of them with high RH expression) are
707 specifically affected by LCC, when compared to HCC (out of 8508 DEGs), as shown by
708 the RNAseq analysis performed on 6 d.o. plants cultivated in liquid medium (mock,
709 LCC, HCC; 24h); 5 genes below the line in the Table are differentially expressed in LCC
710 in comparison to HCC (fold change < 1 = downregulation, fold change > 1 =
711 upregulation).

712

713 **Supplementary figure 1.** A) Cultivation in water does not favour the RH growth and
714 callose deposition; the RH callose reaction requires a rich cultivation medium in order
715 for RHs to grow, and callose deposits to be formed. B) The growth of new RH is
716 inhibited in early time points (4 and 8 h p. t.) in high chitosan concentration (HCC;
717 bars = 100 μm). C) Arabidopsis mutants in secretion, and defence and phytohormone
718 signalling have ability to deposit root hair callose similarly to Col-0. Bars = 100 μm.

719 **Supplementary figure 2**. Actin dynamics is not significantly altered during the early
720 time points of the HCC treatment, as observed using fimbrin-GFP marker and
721 quantified using the variance between the two time points during the observation.

722 **Supplementary figure 3. A)** Numbers of **s**pecific and common DEGs among three
723 different types of experiments with chitosan treatments. B) Cell wall changes triggerd
724 by LCC treatment. Enzymatic fingerprinting of homogalacturonans (upper graph) and
725 xyloglucans (lower graph) from cell walls of WT mock and LCC treated leaves. Data
726 represents mean ±SD, n=4, *P<0.05, **P<0.01, student's t test. OGs are named
727 GalAxMeyAcz. x, y and z indicate the DP and the number of methyl- and acetylester
728 groups, respectively. GalA: Galacturonic acid, Me: methylester group, Ac: Acetylester
729 group. Xyloglucan fragment nomenclature follows that described in Fry et al. (1993):
730 G stands for glucose; X for xylose-glucose; L for galactose-xylose-glucose; F for fucose-
731 galactose-xylose-glucose.

732 **Supplementary figure 4.** Chitosan LCC treatment induces deposition of callose in
733 moss *P. patens* regenerating protoplasts (A) but not in leaf mesophyll-derived
734 Arabidopsis regenerating protoplasts (B), as assayed by aniline blue staining. Bars =
735 100 μm.

736 **Supplemental figure 5** A) LCC has prominent effect on amplification of bacteria *P.*
737 *syringae pv. tomato* (Pst) in flooding experiment *in planta*, as chitosan/LCC added with
738 Pst (chit + Pst) abolishes bacterial amplification in leaf tissue (red arrow points to
739 "null" colony counts), while chitosan pretreatment 24 h prior to Pst inoculation (24 h
740 chit + Pst) causes only small, but significant decrease in colony counts (upper graph);
741 the effect of adding chitosan together with bacteria may not be a direct interference
742 with bacteria amplification, as shown by the experiment of LCC treated Pst *in vitro*
743 (lower graph). B) LCC has a minor effect on auxin signalling enhancement as
744 demonstrated using the DR5::GFP reporter line (bars = 100 μm).

745

746

747

748

749

750

751

752

Bibliography

Aslam SN, Erbs G, Morrissey KL, Newman M-A, Chinchilla D, Boller T, Molinaro A, Jackson RW, Cooper RM. 2009. Microbe-associated molecular pattern (MAMP) signatures, synergy, size and charge: influences on perception or mobility and host defence responses. *Mol Plant Pathol* **10**:375–387. doi:10.1111/j.1364-3703.2009.00537.x

Badri DV, Loyola-Vargas VM, Du J, Stermitz FR, Broeckling CD, Iglesias-Andreu L, Vivanco JM. 2008. Transcriptome analysis of Arabidopsis roots treated with signaling compounds: A focus on signal transduction, metabolic regulation and secretion. *New Phytol* **179**:209–223. doi:10.1111/j.1469-8137.2008.02458.x

Baluška F, Salaj J, Mathur J, Braun M, Jasper F, Šamaj J, Chua NH, Barlow PW, Volkmann D. 2000. Root hair formation: F-actin-dependent tip growth is initiated by local assembly of profilin-supported F-actin meshworks accumulated within expansin-enriched bulges. *Dev Biol* **227**:618–632. doi:10.1006/dbio.2000.9908

Bennett MJ, Marchant A, Green HG, May ST, Ward SP, Millner PA, Walker AR, Schulz B, Feldmann KA. 1996. Arabidopsis AUX1 gene: a permease-like regulator of root gravitropism. *Science* **273**:948–950. doi:10.1126/science.273.5277.948

Brejšková L, Hála M, Rawat A, Soukupová H, Cvrčková F, Charlot F, Nogué F, Haluška S, Žárský V. 2021. SEC6 exocyst subunit contributes to multiple steps of growth and development of Physcomitrella (Physcomitrium patens). *Plant J* **106**:831–843. doi:10.1111/tpj.15205

Brost C, Studtrucker T, Reimann R, Denninger P, Czekalla J, Krebs M, Fabry B, Schumacher K, Grossmann G, Dietrich P. 2019. Multiple cyclic nucleotide-gated channels coordinate calcium oscillations and polar growth of root hairs. *Plant J Cell Mol Biol* **99**:910–923. doi:10.1111/tpj.14371

Cai G, Faleri C, Del Casino C, Emons AMC, Cresti M. 2011. Distribution of callose synthase, cellulose synthase, and sucrose synthase in tobacco pollen tube is controlled in dissimilar ways by actin filaments and microtubules. *Plant Physiol* **155**:1169–1190. doi:10.1104/pp.110.171371

Cao H, Bowling SA, Gordon AS, Dong X. 1994. Characterization of an Arabidopsis Mutant That Is Nonresponsive to Inducers of Systemic Acquired Resistance. *Plant Cell* **6**:1583–1592. doi:10.1105/tpc.6.11.1583

Cao Y, Liang Y, Tanaka K, Nguyen CT, Jedrzejczak RP, Joachimiak A, Stacey G. 2014. The kinase LYK5 is a major chitin receptor in Arabidopsis and forms a chitin-induced complex with related kinase CERK1. *eLife* **3**:e03766. doi:10.7554/eLife.03766

Carol RJ, Dolan L. 2002. Building a hair: tip growth in Arabidopsis thaliana root hairs. *Philos Trans R Soc Lond B Biol Sci* **357**:815–821. doi:10.1098/rstb.2002.1092

Cavalier DM, Lerouxel O, Neumetzler L, Yamauchi K, Reinecke A, Freshour G, Zabotina OA, Hahn MG, Burgert I, Pauly M, Raikhel NV, Keegstra K. 2008. Disrupting two Arabidopsis thaliana xylosyltransferase genes results in plants deficient in xyloglucan, a major primary cell wall component. *Plant Cell* **20**:1519–1537. doi:10.1105/tpc.108.059873

Chin K, DeFalco TA, Moeder W, Yoshioka K. 2013. The Arabidopsis cyclic nucleotide-gated ion channels AtCNGC2 and AtCNGC4 work in the same signaling pathway to regulate pathogen defense and floral transition. *Plant Physiol* **163**:611–624. doi:10.1104/pp.113.225680

Chuberre C, Plancot B, Driouich A, Moore JP, Bardor M, Gügi B, Vicré M. 2018. Plant immunity is compartmentalized and specialized in roots. *Front Plant Sci* **871**:1692–1692. doi:10.3389/fpls.2018.01692

Cove DJ, Perroud P-F, Charron AJ, McDaniel SF, Khandelwal A, Quatrano RS. 2009. Culturing the moss Physcomitrella patens. *Cold Spring Harb Protoc* **2009**:pdb.prot5136. doi:10.1101/pdb.prot5136

Cui W, Lee J-Y. 2016. Arabidopsis callose synthases CalS1/8 regulate plasmodesmal permeability during stress. *Nat Plants* **2**:16034. doi:10.1038/nplants.2016.34

Dehors J, Mareck A, Kiefer-Meyer M-C, Menu-Bouaouiche L, Lehner A, Mollet J-C. 2019. Evolution of Cell Wall Polymers in Tip-Growing Land Plant Gametophytes: Composition, Distribution,

Functional Aspects and Their Remodeling. *Front Plant Sci* **10**:441. doi:10.3389/fpls.2019.00441

Denoux C, Galletti R, Mammarella N, Gopalan S, Werck D, De Lorenzo G, Ferrari S, Ausubel FM, Dewdney J. 2008. Activation of defense response pathways by OGs and Flg22 elicitors in Arabidopsis seedlings. *Mol Plant* **1**:423–445. doi:10.1093/mp/ssn019

Dolan L. 1996. Pattern in the root epidermis: An interplay of diffusible signals and cellular geometry. *Ann Bot* **77**:547–553. doi:10.1006/anbo.1996.0069

Epel BL. 2009. Plant viruses spread by diffusion on ER-associated movement-protein-rafts through plasmodesmata gated by viral induced host beta-1,3-glucanases. *Semin Cell Dev Biol* **20**:1074–1081. doi:10.1016/j.semcdb.2009.05.010

Galway ME, Eng RC, Schiefelbein JW, Wasteneys GO. 2011. Root hair-specific disruption of cellulose and xyloglucan in AtCSLD3 mutants, and factors affecting the post-rupture resumption of mutant root hair growth. *Planta* **233**:985–999. doi:10.1007/s00425-011-1355-6

Gamborg OL, Miller RA, Ojima K. 1968. Nutrient requirements of suspension cultures of soybean root cells. *Exp Cell Res* **50**:151–158. doi:10.1016/0014-4827(68)90403-5

German L, Yeshvekar R, Benitez-Alfonso Y. 2023. Callose metabolism and the regulation of cell walls and plasmodesmata during plant mutualistic and pathogenic interactions. *Plant Cell Environ* **46**:391–404. doi:10.1111/pce.14510

Gómez-Gómez L, Felix G, Boller T. 1999. A single locus determines sensitivity to bacterial flagellin in Arabidopsis thaliana. *Plant J Cell Mol Biol* **18**:277–284. doi:10.1046/j.1365-313x.1999.00451.x

Heisler MG, Ohno C, Das P, Sieber P, Reddy GV, Long JA, Meyerowitz EM. 2005. Patterns of auxin transport and gene expression during primordium development revealed by live imaging of the Arabidopsis inflorescence meristem. *Curr Biol CB* **15**:1899–1911. doi:10.1016/j.cub.2005.09.052

Herburger K, Holzinger A. 2015. Localization and Quantification of Callose in the Streptophyte Green Algae Zygnema and Klebsormidium: Correlation with Desiccation Tolerance. *Plant Cell Physiol* **56**:2259–2270. doi:10.1093/pcp/pcv139

Ichikawa M, Hirano T, Enami K, Fuselier T, Kato N, Kwon C, Voigt B, Schulze-Lefert P, Baluška F, Sato MH. 2014. Syntaxin of plant proteins SYP123 and SYP132 mediate root hair tip growth in Arabidopsis thaliana. *Plant Cell Physiol* **55**:790–800. doi:10.1093/pcp/pcu048

Jacobs AK, Lipka V, Burton RA, Panstruga R, Strizhov N, Schulze-Lefert P, Fincher GB. 2003. An Arabidopsis Callose Synthase, GSL5, Is Required for Wound and Papillary Callose Formation. *Plant Cell* **15**:2503–2513. doi:10.1105/tpc.016097

Jones JDG, Dangl JL. 2006. The plant immune system. *Nature* **444**:323–329. doi:10.1038/nature05286

Keinath NF, Waadt R, Brugman R, Schroeder JI, Grossmann G, Schumacher K, Krebs M. 2015. Live Cell Imaging with R-GECO1 Sheds Light on flg22- and Chitin-Induced Transient [Ca2+]cyt Patterns in Arabidopsis. *Mol Plant* **8**:1188–1200. doi:10.1016/j.molp.2015.05.006

Kemmerling B, Schwedt A, Rodriguez P, Mazzotta S, Frank M, Qamar SA, Mengiste T, Betsuyaku S, Parker JE, Müssig C, Thomma BPHJ, Albrecht C, de Vries SC, Hirt H, Nürnberger T. 2007. The BRI1-associated kinase 1, BAK1, has a brassinolide-independent role in plant cell-death control. *Curr Biol CB* **17**:1116–1122. doi:10.1016/j.cub.2007.05.046

Kentaro Okada, Koei Yachi, Tan Anh Nhi Nguyen, Satomi Kanno, Chika Tateda, Tae-Hong Lee, Uyen Nguyen, Shunsuke Miyashima, Kei Hiruma, Kyoko Miwa, Takaki Maekawa, Michitaka Notaguchi, Yusuke Saijo. 2023. Defense-related callose synthase PMR4 promotes root hair callose deposition and adaptation to phosphate deficiency in Arabidopsis thaliana. *bioRxiv* 2023.07.05.547890. doi:10.1101/2023.07.05.547890

Ks R, Ra L, Rd W, Ha O, A M. 2020. Callose in sporogenesis: Novel composition of the inner spore wall in hornworts. *Plant Syst Evol Entwicklungsgeschichte Syst Pflanz* **306**:16. doi:10.1007/s00606-020-01631-5

Kubátová Z, Pejchar P, Potocký M, Sekereš J, Žárský V, Kulich I. 2019. Arabidopsis Trichome Contains Two Plasma Membrane Domains with Different Lipid Compositions Which Attract Distinct EXO70 Subunits. *Int J Mol Sci* **20**:3803. doi:10.3390/ijms20153803

Kulich I, Vojtíková Z, Glanc M, Ortmannová J, Rasmann S, Žárský V. 2015. Cell wall maturation of Arabidopsis trichomes is dependent on exocyst subunit EXO70H4 and involves callose deposition. *Plant Physiol* **168**:120–131. doi:10.1104/pp.15.00112

Kulich I, Vojtíková Z, Sabol P, Ortmannová J, Neděla V, Tihlaříková E, Žárský V. 2018. Exocyst Subunit EXO70H4 Has a Specific Role in Callose Synthase Secretion and Silica Accumulation. *Plant Physiol* **176**:2040–2051. doi:10.1104/pp.17.01693

Ladwig F, Dahlke RI, Stührwohldt N, Hartmann J, Harter K, Sauter M. 2015. Phytosulfokine regulates growth in arabidopsis through a response module at the plasma membrane that includes cyclic nucleotide-gated channel17, H+-ATPase, and BAK1. *Plant Cell* **27**:1718–1729. doi:10.1105/tpc.15.00306

Lopez-Moya F, Escudero N, Zavala-Gonzalez EA, Esteve-Bruna D, Blázquez MA, Alabadí D, Lopez-Llorca LV. 2017. Induction of auxin biosynthesis and WOX5 repression mediate changes in root development in Arabidopsis exposed to chitosan. *Sci Rep* **7**:16813. doi:10.1038/s41598-017-16874-5

Luna E, Pastor V, Robert J, Flors V, Mauch-Mani B, Ton J. 2011. Callose deposition: a multifaceted plant defense response. *Mol Plant-Microbe Interact MPMI* **24**:183–193. doi:10.1094/MPMI-07-10-0149

Ma X, Wu Y, Zhang G. 2021. Formation pattern and regulatory mechanisms of pollen wall in Arabidopsis. *J Plant Physiol* **260**:153388. doi:10.1016/j.jplph.2021.153388

Meyer D, Pajonk S, Micali C, O'Connell R, Schulze-Lefert P. 2009. Extracellular transport and integration of plant secretory proteins into pathogen-induced cell wall compartments. *Plant J Cell Mol Biol* **57**:986–999. doi:10.1111/j.1365-313X.2008.03743.x

Millet YA, Danna CH, Clay NK, Songnuan W, Simon MD, Werck-Reichhart D, Ausubel FM. 2010. Innate immune responses activated in Arabidopsis roots by microbe-associated molecular patterns. *Plant Cell* **22**:973–990. doi:10.1105/tpc.109.069658

Miya A, Albert P, Shinya T, Desaki Y, Ichimura K, Shirasu K, Narusaka Y, Kawakami N, Kaku H, Shibuya N. 2007. CERK1, a LysM receptor kinase, is essential for chitin elicitor signaling in Arabidopsis. *Proc Natl Acad Sci U S A* **104**:19613–19618. doi:10.1073/pnas.0705147104

Motomura K, Sugi N, Takeda A, Yamaoka S, Maruyama D. 2022. Possible molecular mechanisms of persistent pollen tube growth without de novo transcription. *Front Plant Sci* **13**:1020306. doi:10.3389/fpls.2022.1020306

Ngou BPM, Ahn H-K, Ding P, Jones JDG. 2021. Mutual potentiation of plant immunity by cell-surface and intracellular receptors. *Nature* **592**:110–115. doi:10.1038/s41586-021-03315-7

Okada K, Kubota Y, Hirase T, Otani K, Goh T, Hiruma K, Saijo Y. 2021. Uncoupling root hair formation and defence activation from growth inhibition in response to damage-associated Pep peptides in Arabidopsis thaliana. *New Phytol* **229**:2844–2858. doi:10.1111/nph.17064

Ortmannová J, Sekereš J, Kulich I, Šantrůček J, Dobrev P, Žárský V, Pečenková T. 2022. Arabidopsis EXO70B2 exocyst subunit contributes to papillae and encasement formation in antifungal defence. *J Exp Bot* **73**:742–755. doi:10.1093/jxb/erab457

Park K, Jang BK, Lee HM, Cho JS, Lee CH. 2020. An Efficient Method for In Vitro Shoot-Tip Culture and Sporophyte Production Using Selaginella martensii Spring Sporophyte. *Plants Basel Switz* **9**:235. doi:10.3390/plants9020235

Park S, Szumlanski AL, Gu F, Guo F, Nielsen E. 2011. A role for CSLD3 during cell-wall synthesis in apical plasma membranes of tip-growing root-hair cells. *Nat Cell Biol* **13**:973–980. doi:10.1038/ncb2294

Parker JS, Cavell AC, Dolan L, Roberts K, Grierson CS. 2000. Genetic interactions during root hair morphogenesis in Arabidopsis. *Plant Cell* **12**:1961–1974. doi:10.1105/tpc.12.10.1961

Paterlini A, Sechet J, Immel F, Grison MS, Pilard S, Pelloux J, Mouille G, Bayer EM, Voxeur A. 2022. Enzymatic fingerprinting reveals specific xyloglucan and pectin signatures in the cell wall purified with primary plasmodesmata. *Front Plant Sci* **13**.

Pečenková T, Janda M, Ortmannová J, Hajná V, Stehlíková Z, Žárský V. 2017. Early Arabidopsis root hair growth stimulation by pathogenic strains of Pseudomonas syringae. *Ann Bot* **120**:437–

446. doi:10.1093/aob/mcx073
Porter K, Day B. 2016. From filaments to function: The role of the plant actin cytoskeleton in pathogen perception, signaling and immunity. *J Integr Plant Biol* **58**:299–311. doi:10.1111/jipb.12445
Radin I, Richardson RA, Coomey JH, Weiner ER, Bascom CS, Li T, Bezanilla M, Haswell ES. 2021. Plant PIEZO homologs modulate vacuole morphology during tip growth. *Science* **373**:586–590. doi:10.1126/science.abe6310
Rentel MC, Lecourieux D, Ouaked F, Usher SL, Petersen L, Okamoto H, Knight H, Peck SC, Grierson CS, Hirt H, Knight MR. 2004. OXI1 kinase is necessary for oxidative burst-mediated signalling in Arabidopsis. *Nature* **427**:858–861. doi:10.1038/nature02353
Rich-Griffin C, Eichmann R, Reitz MU, Hermann S, Woolley-Allen K, Brown PE, Wiwatdirekkul K, Esteban E, Pasha A, Kogel KH, Provart NJ, Ott S, Schäfer P. 2020. Regulation of cell type-specific immunity networks in arabidopsis roots. *Plant Cell* **32**:2742–2762. doi:10.1105/TPC.20.00154
Ringli C, Baumberger N, Diet A, Frey B, Keller B. 2002. ACTIN2 is essential for bulge site selection and tip growth during root hair development of Arabidopsis. *Plant Physiol* **129**:1464–1472. doi:10.1104/pp.005777
Serre NBC, Kralík D, Yun P, Slouka Z, Shabala S, Fendrych M. 2021. AFB1 controls rapid auxin signalling through membrane depolarization in Arabidopsis thaliana root. *Nat Plants* **7**:1229–1238. doi:10.1038/s41477-021-00969-z
Shih HW, Depew CL, Miller ND, Monshausen GB. 2015. The cyclic nucleotide-gated channel CNGC14 regulates root gravitropism in arabidopsis thaliana. *Curr Biol* **25**:3119–3125. doi:10.1016/j.cub.2015.10.025
Sun H, Zhu X, Li C, Ma Z, Han X, Luo Y, Yang L, Yu J, Miao Y. 2021. Xanthomonas effector XopR hijacks host actin cytoskeleton via complex coacervation. *Nat Commun* **12**:4064. doi:10.1038/s41467-021-24375-3
Suwanchaikasem P, Idnurm A, Selby-Pham J, Walker R, Boughton BA. 2022. Root-TRAPR: a modular plant growth device to visualize root development and monitor growth parameters, as applied to an elicitor response of Cannabis sativa. *Plant Methods* **18**:46. doi:10.1186/s13007-022-00875-1
Vaškebová L, Šamaj J, Ovecka M. 2018. Single-point ACT2 gene mutation in the Arabidopsis root hair mutant der1-3 affects overall actin organization, root growth and plant development. *Ann Bot* **122**:889–901. doi:10.1093/aob/mcx180
Verma DP, Hong Z. 2001. Plant callose synthase complexes. *Plant Mol Biol* **47**:693–701. doi:10.1023/a:1013679111111
Vissenberg K, Claeijs N, Balcerowicz D, Schoenaers S. 2020. Hormonal regulation of root hair growth and responses to the environment in Arabidopsis. *J Exp Bot* **71**:2412–2427. doi:10.1093/JXB/ERAA048
Vogel J, Somerville S. 2000. Isolation and characterization of powdery mildew-resistant Arabidopsis mutants. *Proc Natl Acad Sci U S A* **97**:1897–1902. doi:10.1073/pnas.030531997
Voxeur A, Habrylo O, Guénin S, Miart F, Soulié M-C, Rihouey C, Pau-Roblot C, Domon J-M, Gutierrez L, Pelloux J, Mouille G, Fagard M, Höfte H, Vernhettes S. 2019. Oligogalacturonide production upon Arabidopsis thaliana-Botrytis cinerea interaction. *Proc Natl Acad Sci U S A* **116**:19743–19752. doi:10.1073/pnas.1900317116
Wan J, Tanaka K, Zhang X-C, Son GH, Brechenmacher L, Nguyen THN, Stacey G. 2012. LYK4, a lysin motif receptor-like kinase, is important for chitin signaling and plant innate immunity in Arabidopsis. *Plant Physiol* **160**:396–406. doi:10.1104/pp.112.201699
Wang X, Wang K, Yin G, Liu X, Liu M, Cao N, Duan Y, Gao H, Wang W, Ge W, Wang J, Li R, Guo Y. 2018. Pollen-Expressed Leucine-Rich Repeat Extensins Are Essential for Pollen Germination and Growth. *Plant Physiol* **176**:1993–2006. doi:10.1104/pp.17.01241
Wang Y-S, Motes CM, Mohamalawari DR, Blancaflor EB. 2004. Green fluorescent protein fusions to Arabidopsis fimbrin 1 for spatio-temporal imaging of F-actin dynamics in roots. *Cell Motil*

Cytoskeleton **59**:79–93. doi:10.1002/cm.20024

Ye W, Munemasa S, Shinya T, Wu W, Ma T, Lu J, Kinoshita T, Kaku H, Shibuya N, Murata Y. 2020. Stomatal immunity against fungal invasion comprises not only chitin-induced stomatal closure but also chitosan-induced guard cell death. *Proc Natl Acad Sci U S A* **117**:20932–20942. doi:10.1073/pnas.1922319117

Yoo S-D, Cho Y-H, Sheen J. 2007. Arabidopsis mesophyll protoplasts: a versatile cell system for transient gene expression analysis. *Nat Protoc* **2**:1565–1572. doi:10.1038/nprot.2007.199

Yuan P, Jauregui E, Du L, Tanaka K, Poovaiah BW. 2017. Calcium signatures and signaling events orchestrate plant–microbe interactions. *Curr Opin Plant Biol* **38**:173–183. doi:10.1016/j.pbi.2017.06.003

Zamioudis C, Mastranesti P, Dhonukshe P, Blilou I, Pieterse CMJ. 2013. Unraveling root developmental programs initiated by beneficial Pseudomonas spp. Bacteria. *Plant Physiol* **162**:304–318. doi:10.1104/pp.112.212597

Zhang J, Li Y, Bao Q, Wang H, Hou S. 2022. Plant elicitor peptide 1 fortifies root cell walls and triggers a systemic root-to-shoot immune signaling in Arabidopsis. *Plant Signal Behav* **17**:2034270. doi:10.1080/15592324.2022.2034270

Zhang M, Zhang S. 2022. Mitogen-activated protein kinase cascades in plant signaling. *J Integr Plant Biol* **64**:301–341. doi:10.1111/jipb.13215

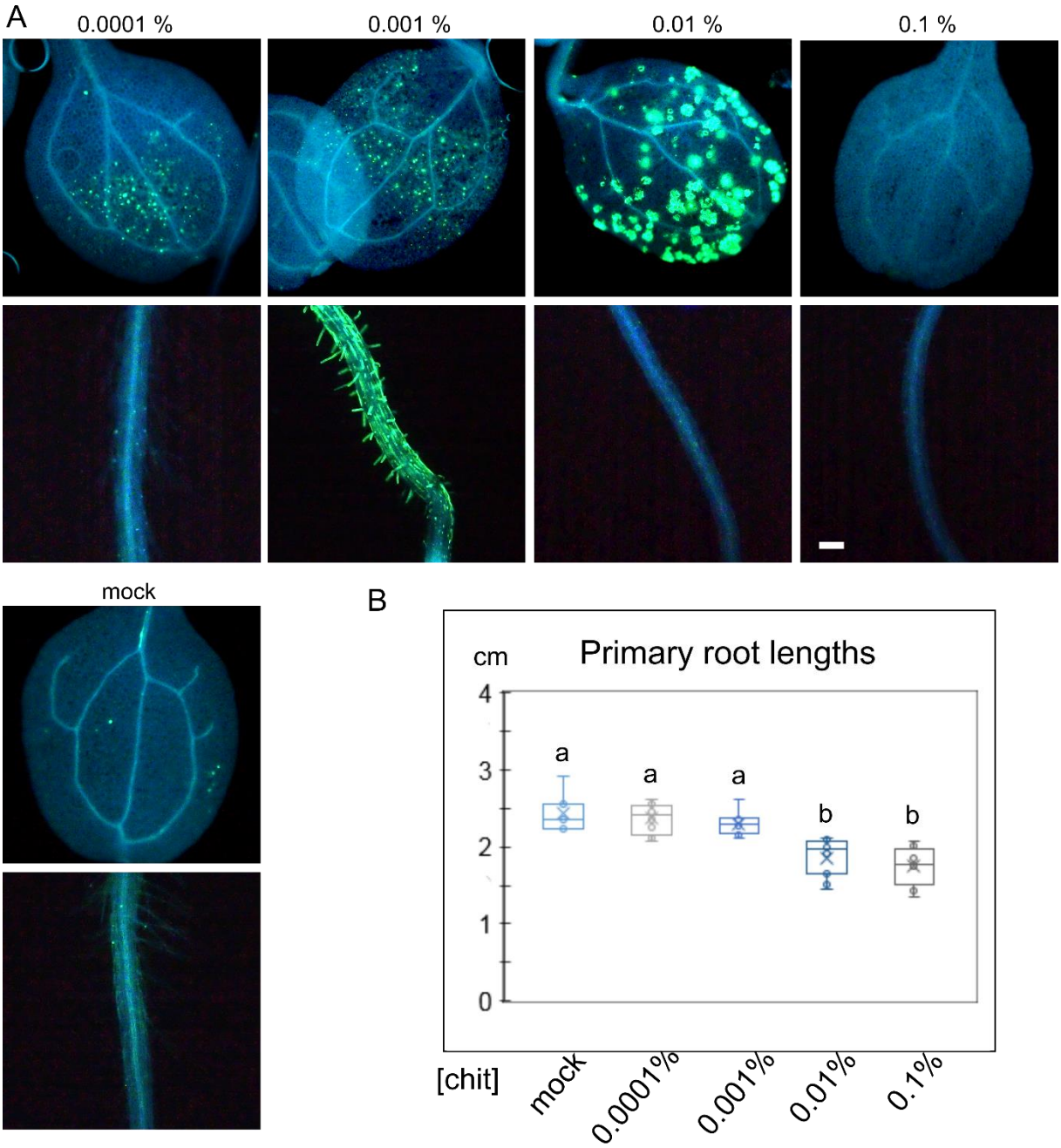

Figure 1. Concentration dependent modes of chitosan-triggered callose deposition. Different concentrations of chitosan cause different patterns of callose depositions 24 h post treatment (p. t.) in both cotyledons and roots (root hairs); mock treatment as a control below (bar = 100 μm). B) Concentration dependent primary root growth inhibition 24 h p. t. Small letters indicate significance of differences based on the ANOVA test.

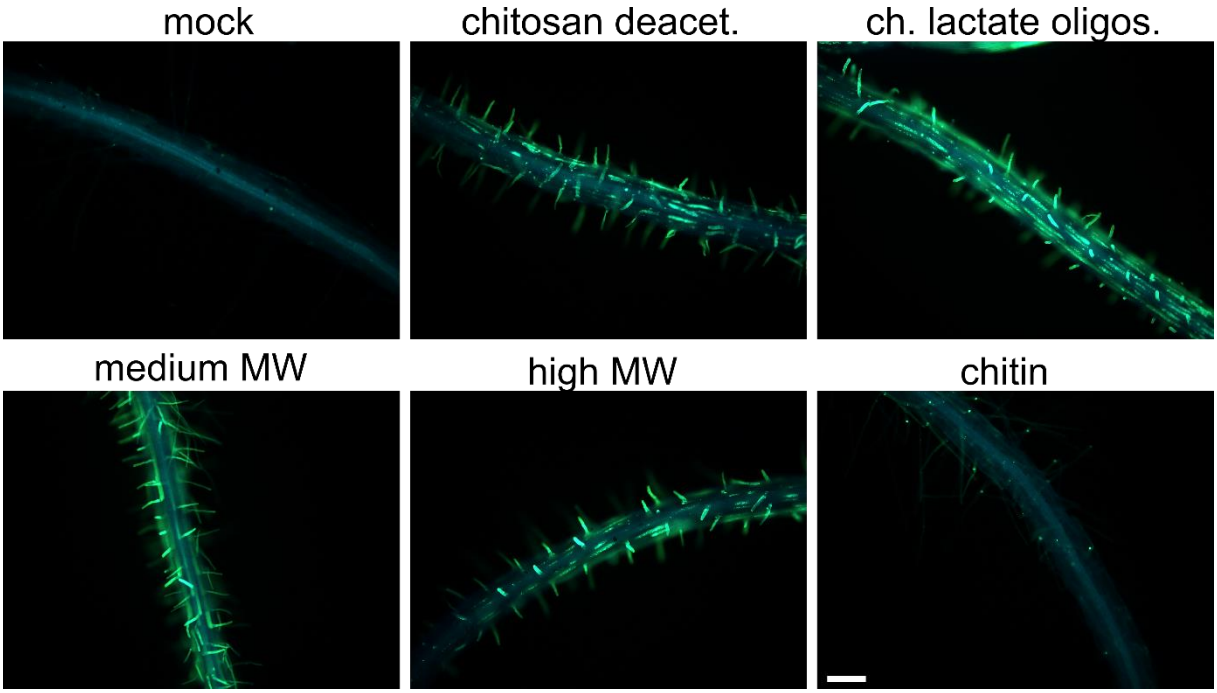

Figure 2. Root hair growth during the chitosan treatments. A) The low chitosan concentration (0.001%, LCC) of several other chitosan variants has the same effect on RH callose deposition (bar = 100 μm).

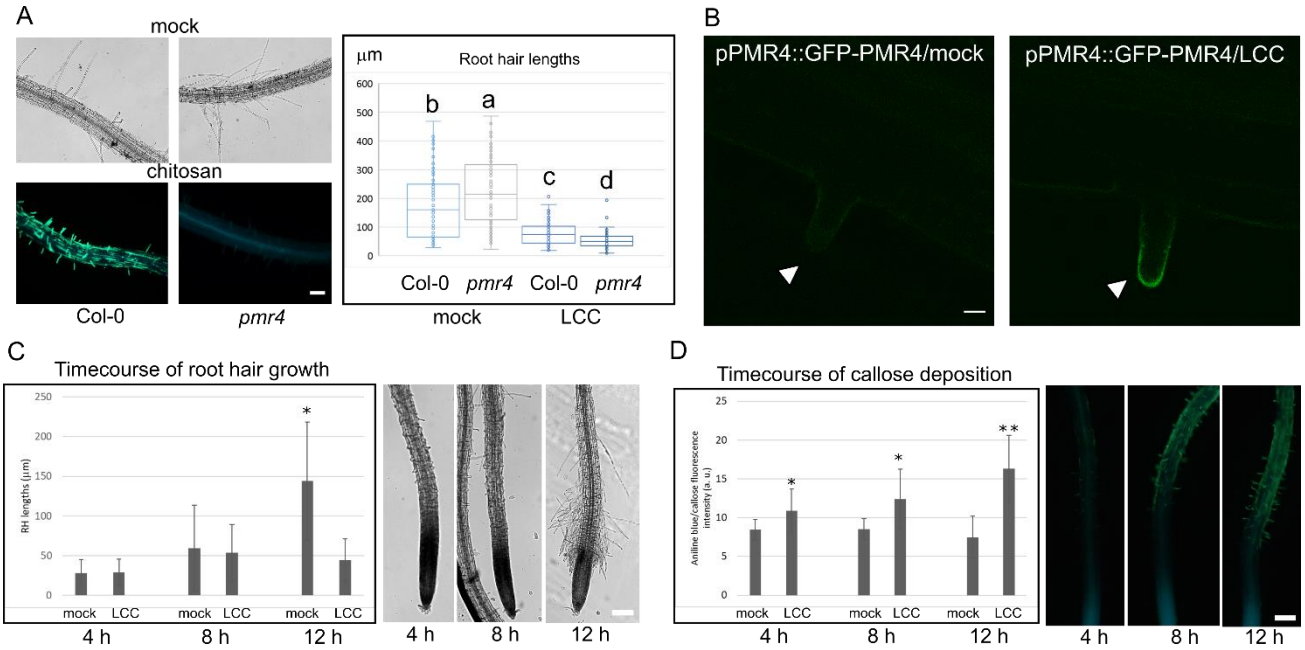

Figure 3. Callose deposition in LCC is PMR4-dependent. A) A *pmr4* mutant root hair (RH) growth does not deposit callose upon the LCC treatment; nevertheless, the RH growth is suppressed to the similar extent as in the Col-0 control. Small letters indicate significance of differences based on the ANOVA test. B) Upon the LCC treatment, at 4 h p. t. GFP-PMR4 accumulates on the tips of growing RH, further confirming a role for PMR4 in RHs callose deposition (marked by white asterisks). C) The time course of decline of the RH growth during the LCC treatment; the significant growth inhibition is observable at 12 h p.t. D) Timecourse of callose deposition reveals significant changes between the mock and LCC already at 4 h p. t. Bars = 100 µm in A), C) and D) and 10 µm in B).

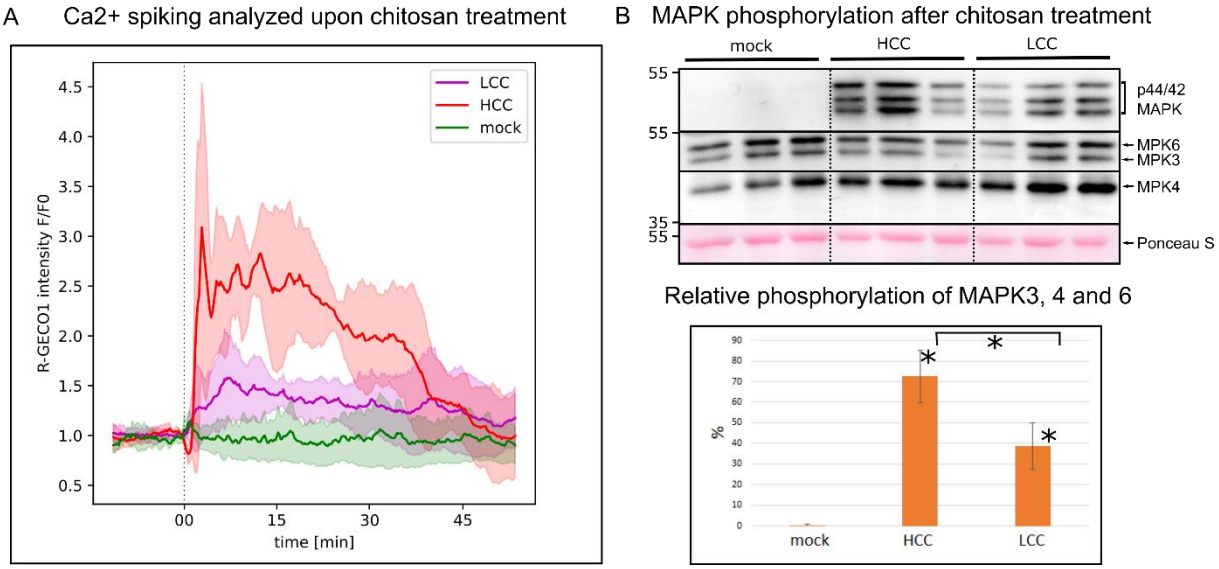

Figure 4. Chitosan-triggered signalling in *A. thaliana* seedlings. A) Ca^{2+} spiking analysed as R-GECO sensor fluorescence in root cells upon chitosan treatment shows slightly later onset with mild oscillations and long duration within the ca 45 min frame of LCC treatment, while HCC induces prominent Ca^{2+} spiking with subsequent drop in signal intensity. B) Western blot analysis of MAPK activation by phosphorylation upon 30 min of HCC and LCC treatments quantified as the ratio of band intensities obtained for phosphorylated portion versus the whole pool MAPKs. Both treatments cause significant increase in MPK3/6/4 phosphorylation in comparison to the mock treatment, also the difference between the LCC- and HCC-caused phosphorylations is significant, with LCC causing almost two-time less MAPKs phosphorylation.

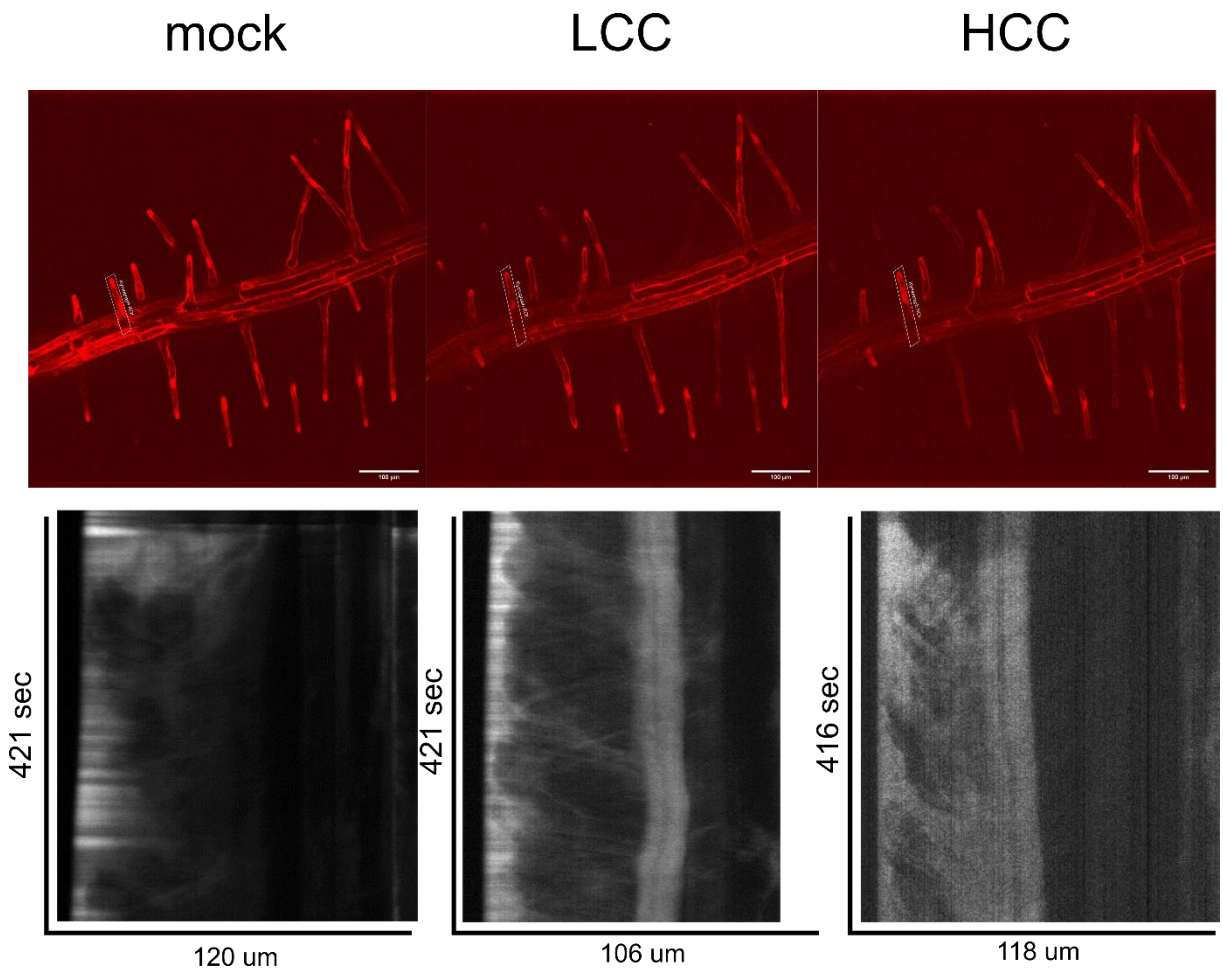

Figure 5. R-GECO signal patterns upon mock, LCC and HCC treatment; below are kymographs showing R-GECO dynamics within the selected RH (white rectangles in upper row) in a time range of approximately 7 min after treatments; bars = 100 μm.

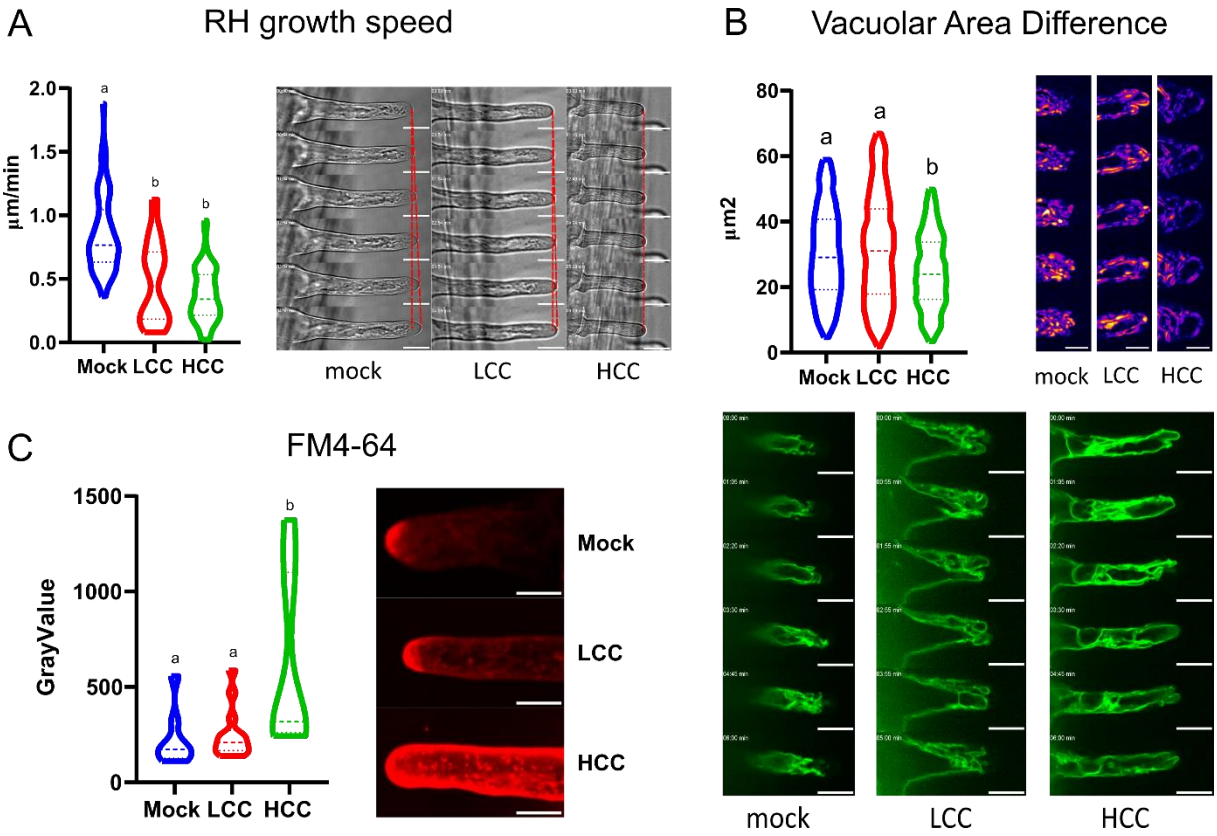

Figure 6. Subcellular dynamics during the early time points of LCC and HCC treatments. A) The real-time analysis of the root hairs growth during the mock, LCC, and HCC treatments based on the bright field images. The plot shows the RH growth rates for the mock, LCC and HCC treatments; small letters indicate significant differences based on Kruskal - Wallis test. B) The real-time changes in the vacuolar dynamics quantified as a vacuole-occupied area in the RH tip, imaged using the tonoplast marker Vti-GFP. The plot displays the differences between two consecutive frames; the examples of the differential signal are shown on the right; examples of vacuolar dynamics are shown below. Small letters indicate significant differences based on the ANOVA test. Bar = 20 µm. C) The analyses of the endocytosed FM4-64 dye after 15 min of treatments for mock, LCC, and HCC. The endocytic compartment stained by FM4-64 in the RH tip area is prominently enhanced in case of the HCC treatments. Small letters indicate significant differences based on Kruskal -Wallis test. On the right are examples of maximal intensity projections of FM4 -64 stained root hairs. Bar = 10 µm.

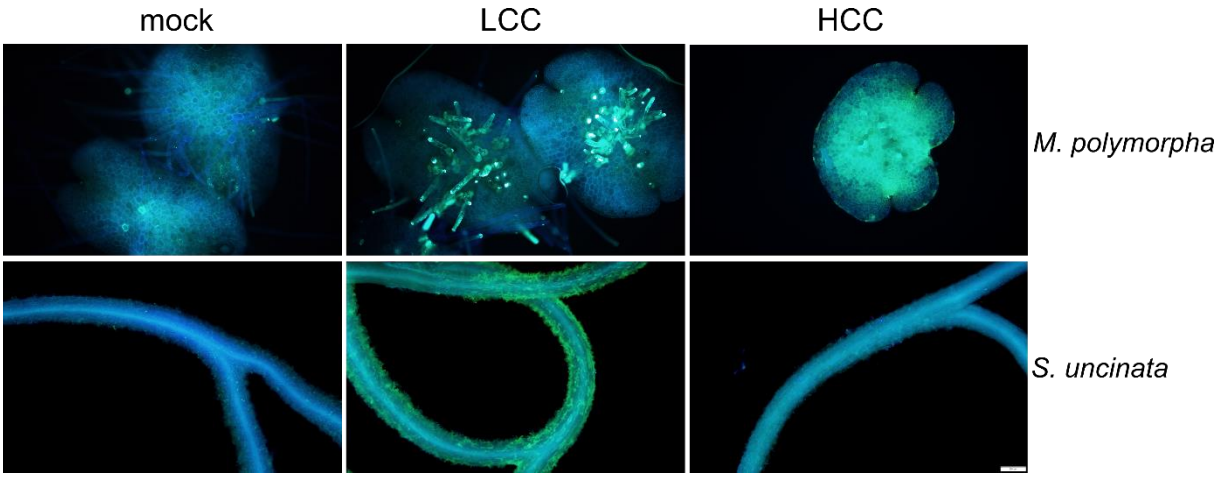

Figure 7. Callose deposition is conserved in structures analogous to root hairs. *M. polymorpha (liverwort)* rhizoids growing out of gemma are enclosed by callose when incubated for 24 h with LCC. The same effect is observable also on spikemoss rhizophores (*S. uncinata*). Bar = 100 μm.

Table I. Eleven genes (out of 59 DEGS; most of them with good RH expression) are specifically affected by LCC, when compared to HCC chitosan treatment (out of 8508 DEGs); 5 genes below the line in the Table are differentially expressed in LCC in comparison to HCC (fold change < 1 = downregulation, fold change > 1 = upregulation).

gene identifier	gene name	protein function	fold change LCC	fold change HCC
AT1G72900	ERF11	ERF domain protein 11	0.49	insig.
AT2G22500	DIC1	uncoupling protein 5	0.59	insig.
AT2G46400	WRKY46	DNA-binding protein 46	0.36	insig.
AT3G22800		leucine-rich repeat (LRR)/extensin	1.85	insig.
AT3G56400	WRKY70	WRKY DNA-binding protein 70	0.48	insig.
AT4G08950	EXO	phosphate-responsive 1 family protein	0.70	insig.
AT4G11280	ACS6	1-aminocyclopropane-1-carboxylic acid (ACC) synthase 6	0.47	insig.
AT4G24380		involved in 10-formyltetrahydrofolate biosynthesis	0.42	insig.
AT5G41750		disease resistance protein (TIR-NBS-LRR class) family	0.42	insig.
AT5G59550		zinc finger (C3HC4-type RING finger) family protein	0.63	insig.
AT5G64870		SPFH/Band 7/PHB domain-containing, flotillin	0.49	insig.
AT1G72900		Toll-Interleukin-Resistance (TIR) domain-containing protein	0.57	2.95
AT2G16660		major facilitator superfamily protein	0.52	1.30
AT2G34930		disease resistance family protein LRR	0.62	1.79
AT3G50930	BCS1	cytochrome BC1 synthesis	0.44	2.12
AT5G42380	CML37	calmodulin like 37	0.32	2.50